Experiments in Fluids 35 (2003) 24–31
DOI 10.1007/s00348-003-0609-x

Schlieren measurement of axisymmetric internal wave amplitudes

K. Onu, M.R. Flynn, B.R. Sutherland

Abstract "Synthetic schlieren", which has been used to measure the amplitude of two-dimensional internal wave beams generated from an oscillating cylinder, is adapted to analyze axisymmetric internal waves generated by an oscillating sphere. This nonintrusive technique uses elementary inverse tomographic methods to measure the amplitude of the conical-structured wave beams everywhere in space and time. We compare the results with in situ probe measurements, and we examine the structure of the wave beams generated by a sphere oscillating at different amplitudes.

1 Introduction

Internal waves generated from a periodically oscillating sphere are well known to propagate along wave beams with fixed angle to the vertical (Mowbray and Rarity 1967; Lighthill 1978). Specifically, inviscid linear theories predict the waves propagate with the structure of two cones one lying above and the other below the sphere. The waves have a horizontal cross-sectional area that increases linearly with vertical distance from the source, and conservation of energy flux therefore requires that the amplitude decreases as $r^{-1/2}$, where r is the radial distance from the centre of the sphere (Appleby and Crighton 1987; Voisin 1991). A failing of inviscid theory is that it predicts unphysically large velocities where the wave beams are tangent to the sphere. Although this can be rectified by including viscous effects (B. Voisin, private communication), the dynamics of the coupling with the waves to the viscous boundary layer surrounding the sphere remain poorly understood.

Received: 4 March 2002 / Accepted: 14 February 2003
Published online: 20 May 2003
© Springer-Verlag 2003

K. Onu, M.R. Flynn, B.R. Sutherland (✉)
Dept. of Mathematical and Statistical Sciences,
University of Alberta,
Edmonton, AlbertaT6G 2G1, Canada
Email: bruce.sutherland@ualberta.ca

We are grateful to S. Dalziel and G. Hughes for their insights during the initial stages of this work. This work was supported by funding from the Natural Sciences and Engineering Research Council (NSERC) of Canada, Grant No. 203065-00, and NSERC's USRA program

In order to gain insight into these dynamics through laboratory experiments, we adapted a recently developed schlieren technique in order to measure the amplitude of axisymmetric internal waves generated by an oscillating sphere. Schlieren techniques, which exploit how light rays are bent as they pass through a density gradient, have often been used to observe the structure of internal waves. The techniques have the advantage of being nonintrusive and sensitive to small disturbances in stratified fluids (Mowbray 1967; Stevenson 1969).

Classical schlieren techniques are useful as a qualitative tool, enabling one to visualise wave crests and troughs, but providing no amplitude information. Quantitative schlieren methods have been developed in the past decade with the aid of digital enhancement (Irvin and Ross 1991; Greenberg et al. 1995; Dalziel et al. 2000). "Synthetic schlieren" has proven particularly useful for measuring the amplitude of waves generated by an oscillating circular and elliptical cylinder (Sutherland et al. 1999, 2000; Sutherland and Linden 2002). In these experiments a camera is focussed through a stratified saltwater solution upon an object image of horizontal black lines. Internal waves are generated from an oscillating cylinder that spans the tank with its axis along the line of sight of the camera. The waves stretch and compress isopycnal (constant density) surfaces, thus bending the light reaching the camera and distorting the object image. Knowing the linear relationship between density and the index of refraction of salt water (Weast 1981), and assuming the wave beams are uniform along the line of sight of the camera, the amplitude of the waves is easily calculated from the measured displacement of lines in the distorted object image.

Here matrix inversion methods are employed to adapt synthetic schlieren to measure axisymmetric internal wave fields. To illustrate the validity and practical use of the technique, we perform a series of laboratory experiments in which internal waves are generated by a vertically oscillating sphere in uniformly stratified fluid.

The experimental setup and the qualitative use of synthetic schlieren is described in Sect. 2. In Sect. 3 we describe how the wave amplitudes are determined from the measured distortion of an object image behind the tank. The techniques are applied to the experimental data in Sect. 4. We summarise our results in Sect. 5.

2 Experimental set-up

The experiments are performed in an approximately cubical acrylic tank having internal measurements of

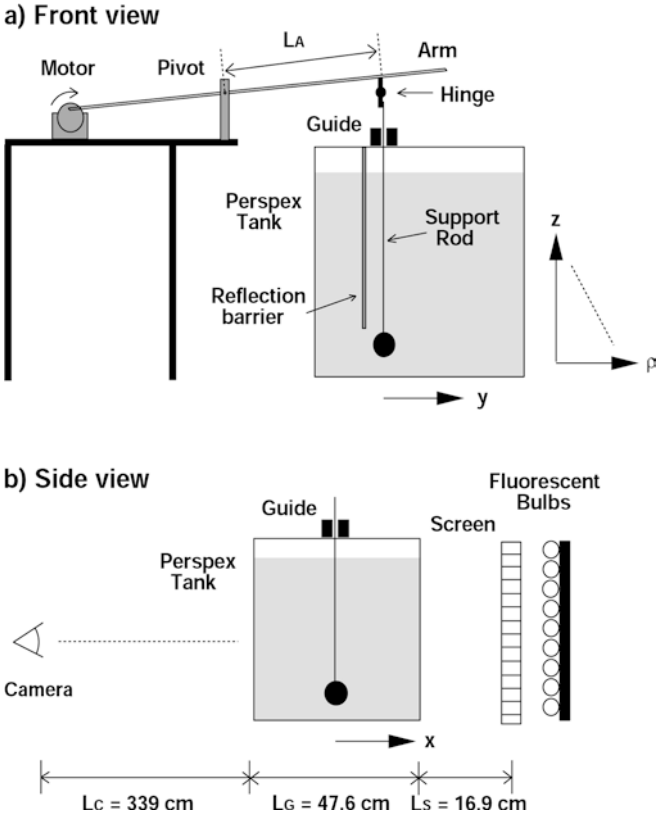

Fig. 1. a) Front view of the tank showing the oscillating cylinder mechanism. **b)** Side view (not to scale) of the tank showing the relative position of the tank to the CCD camera

height H=48.6 cm, length L_0=47.6 cm and width L_t=47.7 cm. The tank is filled to a depth of 44.3 cm with a uniformly stratified salt solution using a "double bucket" system (Oster 1965). A traversing 50 cm long fast conductivity and temperature probe (Precision Measurement Engineering, USA) is used to measure conductivity and hence density ρ as a function of depth. Thus we are able to determine the background-squared buoyancy frequency, defined in the Boussinesq approximation by $N_0^2=-(g/\rho_0)\mathrm{d}\rho/\mathrm{d}z$, in which g is the acceleration of gravity, and ρ_0 is the characteristic density of water. Explicitly, the buoyancy frequency is determined from the slope of the best-fit line through $\rho(z)$. Typical experiments have N_0=0.99±0.02 s^{-1}.

The conductivity probe is also used to measure conductivity variations at a fixed point in order to provide a secondary check on synthetic schlieren measurements. These measurements accurately measure density variations in time to a resolution of 0.00004 g/cm^3.

Internal waves are generated by a vertically oscillating plastic sphere of radius a=3.2 cm. The hollow sphere is filled with a saltwater solution so that it is almost neutrally buoyant when suspended underwater. As shown in Fig. 1, the sphere is attached to a thin metal rod, the other end of which is connected through a hinge to a sinusoidally oscillating arm. In each case, the rod is passed through a narrow guide placed across the top of the tank thus ensuring that the sphere's motion is vertical. A "reflection barrier" is positioned above and to the left of the sphere in the tank. This acts to inhibit initial interference from reflected waves on the opposite side of the upward propagating wave cone.

The frequency of oscillation is controlled by adjusting the rate of rotation of the motor. For the present study, an angular frequency of ω=0.49 s^{-1} is selected for all runs. This frequency was chosen so that waves emanate away from the sphere at an angle to the vertical of $\Theta=\cos^{-1}(\omega/N_0)\simeq 60°$, thus inhibiting interference of the wave beam in the upper right-hand quadrant of the field of view with the wave beams in the other sectors. The amplitude of oscillation is controlled by altering L_A, the distance between the arm's pivot point and the position of the hinge, as shown in Fig. 1a. Here we examine waves generated by the sphere oscillating with peak-to-peak amplitudes $2A$=1.74, 1.18 and 0.64 cm. Even for those runs involving the largest amplitude of oscillation, the flow around the sphere is observed to be laminar. The internal wave field is visualised by employing a synthetic schlieren system (Sutherland et al. 1999), of which only the relevant features are summarised here.

The set-up of synthetic schlieren is shown in Fig. 1b. A translucent screen of evenly spaced 0.25-cm thick horizontal black lines is placed L_s=16.9 cm behind the tank. The screen is illuminated from behind by a rack of fluorescent bulbs. The experiment is recorded on digital tape by a CCD camera positioned approximately L_c=339 cm in front of the tank. In order to capture as much of the wave beam as possible, the sphere is situated towards the tank's lower left-hand corner with the camera's field of view centred in the upper right-hand quadrant of the resulting wave field.

The camera is connected to a computer running DigImage (Dalziel 1992), a robust image retrieval and enhancement software package. Specifically, DigImage is used to convert snapshots and time series images of the experiment into matrices of data. The value of each matrix element is linearly related to the average intensity of light incident upon the corresponding pixel area. In typical snapshot images, the pixel area is 0.05×0.05 cm^2. In time series images, the temporal resolution can be as small as Δt=1/30 s.

Internal waves may be visualised in real time using DigImage. This is illustrated in Fig. 2, which shows digital snapshots taken immediately before (Fig. 2a) and during (Fig. 2b) an experiment. In both, the sphere is situated in the bottom left-hand corner and the camera is looking through the stratified fluid in the tank to the object image of horizontal black and white lines behind the tank. The snapshot in Fig. 2b is taken after two complete oscillations of the sphere and shows a distorted object image.

Light is bent to a greater degree as it passes through a stronger density gradient. Therefore a light ray that passes from a point on the object image through the undisturbed fluid in the tank to the camera will instead emanate from a lower point on the object image if it passes through a region where isopycnals are compressed by internal waves. So the object image will appear to shift upward. Conversely, the object image will appear to shift downward when viewed through isopycnal surfaces that are stretched apart.

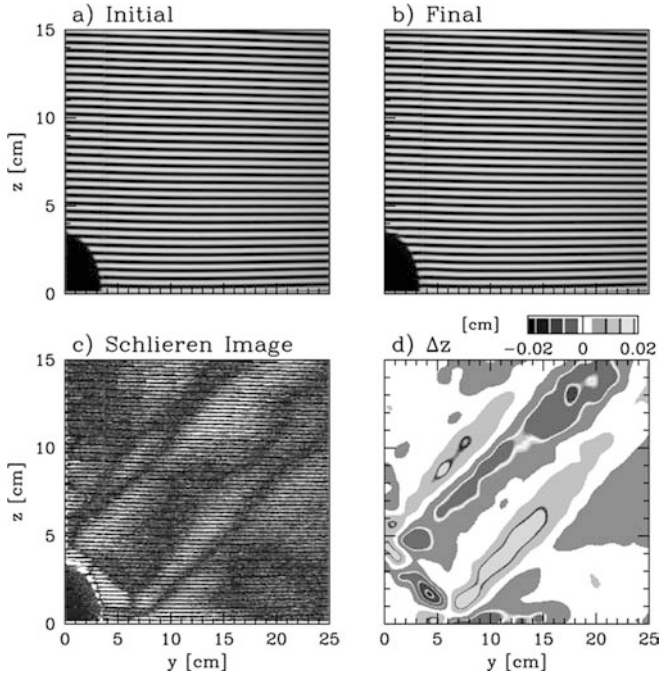

Fig. 2a–d. Snapshots from experiment (**a**) prior to oscillation and (**b**) at the beginning of the third oscillation with $2A$=1.74 cm. Taking the difference between (a) and (b) and multiplying by an enhancement factor of 5 yields (**c**), the synthetic schlieren image. The corresponding Δz field is shown in (**d**)

Although the snapshots in Fig. 2a and 2b are virtually indistinguishable to the naked eye (except near the sphere itself), the distortion can be enhanced by taking the difference between the two snapshots and multiplying the result by a constant "enhancement factor". The resulting "qualitative synthetic schlieren image" (Fig. 2c) clearly reveals the presence of a coherent wave beam propagating upward and to the right of the sphere.

Through interpolation, the apparent vertical displacement because of the bending of light rays can be measured with an accuracy typically as small as 0.002 cm. The interpolation is performed accurately only for pixels corresponding to the edges of the dark lines on the object image. Displacements corresponding to the center of the light and dark lines are found by a Gaussian weighted average of the displacements at the edges of the lines. The resulting matrix of displacement values is then put through a low pass filter to reduce noise (Sutherland et al. 1999). One thereby obtains the field corresponding to the object image's vertical displacement, $\Delta z(y,z)$, as shown in Fig. 2d. Here the maximum vertical displacement is one tenth the width of one of lines on the original object image, but ten times larger than the smallest resolvable displacement.

It is interesting to note that values of Δz do not decrease as the square root of the distance from the sphere. Although the wave amplitude decreases at this rate, the distance over which the light ray passes through a region distorted by an axisymmetric wave field increases linearly with r. Fortuitously, this means the signal remains strong even far from the sphere.

In Sect. 3, we show how inverse tomography methods are used to calculate from Δz the change in the density gradient due to an axisymmetric wave field. Ultimately, from this field and its time derivative, one can calculate such useful wave fields as the velocity and vertical displacement of fluid due to waves.

3
Determination of wave amplitudes

In order to determine density gradient fluctuations from the apparent displacement Δz of points in an object image viewed through the tank, we first determine how a light ray is bent due to the compression and stretching of isopycnal surfaces. By relating the deviation of the light ray to the observed displacements and assuming the waves are axisymmetric, the resulting matrix equation can be inverted to give values of the wave amplitude everywhere in space.

3.1
Deflection of a light ray in a stratified fluid

Because the index of refraction of salt water is almost linearly related to change in salinity, light rays bend to different degrees depending upon the density gradient in a stratified fluid. Snell's law describes how a light ray bends at the interface of two media with different refractive indices n. Explicitly,

$$n \sin\theta = \text{constant}. \tag{1}$$

Here θ is the angle between the path of the light ray and the vertical both above and below the unperturbed interface. Equation (1) generalizes to continuously stratified media by writing the equation in differential form

$$\frac{\mathrm{d}\theta}{\mathrm{d}n} = -\frac{\tan\theta}{n}. \tag{2}$$

In general, to find ray paths in a stratified fluid we would treat n and θ as functions of along-tank (x), across-tank (y) and vertical (z) coordinates (Fig. 1). However, because the synthetic schlieren system used here detects apparent vertical displacements of horizontal lines, deflections in the y-direction, which are small in any case, are not measured. Thus we consider only the dependence of n and θ upon x and z. Applying the chain rule and the trigonometric relation $\mathrm{d}x/\mathrm{d}z=\theta$ to the left side of n we obtain

$$\frac{\partial\theta}{\partial x}\left[\frac{\mathrm{d}x}{\mathrm{d}n} + \frac{\mathrm{d}z}{\mathrm{d}n}\tan\theta\right] = -\frac{\tan\theta}{n}. \tag{3}$$

Because the light passes from the object image to the camera along approximately horizontal rays, further progress can be made by a using a Taylor series expansion with $\theta \simeq \pi/2$. Thus Eq. (3) becomes

$$z''\left(z'\frac{1}{\partial n/\partial x} + \frac{1}{\partial n/\partial z}\right) = \frac{1}{n}, \tag{4}$$

in which primes denote derivatives with respect to x. Given a disturbance to the refractive index field $n(x,z)$, Eq. (4) describes the path $z(x)$ of the light ray through the tank. The nonlinear ordinary differential equation is further simplified by supposing, consistent with the approximation $\theta \simeq \pi/2$, that the light ray traverses only a small vertical distance (typically less than 1 cm) as it

passes through the tank. We therefore assume a locally linear dependence of n on z. Explicitly,

$$n(x,z) = \alpha_0(x) + \alpha_1(x)z. \tag{5}$$

In the x-direction, internal waves may produce increasing and decreasing refractive index changes along the path of the light ray, so the x-dependence is left unspecified. Since α_0 is the leading-order term of the refractive index, $O(\alpha_0)=n_0\simeq 1.3330$ (for water). The value of α_1 is related to the squared buoyancy frequency by $\alpha_1=\partial n/\partial z\simeq -\gamma n_0 N^2$, where

$$\gamma = \frac{1}{9}\frac{\rho_0}{n_0}\frac{\Delta n}{\Delta \rho} \simeq 1.878\times 10^{-4}\ \mathrm{s^2/cm}.$$

Here we use the fact that the density of salt water changes approximately linearly with refractive index (Weast 1981) as $\Delta\rho/\Delta n\simeq 4.07\ \mathrm{g/cm^3}$.

In our experiments $O(N)=O(N_0)=1\ \mathrm{s^{-1}}$ and $O(\delta z)=1$ cm. These physical considerations show that $|\alpha_1\delta z/\alpha_0|\ll 1$ and $|x'_1\delta z/\alpha'_0|\ll 1$. Thus, substituting Eq. (5) into Eq. (4), and keeping only low-order terms in α_1/α_0 gives

$$z'' + \left(\frac{\alpha_1}{\alpha_0}\right)^2 z - z''z'z\frac{\alpha_1\alpha'_1}{(\alpha'_0)^2} + z''z'\frac{\alpha_1}{\alpha'_0} = \frac{\alpha_1}{\alpha_0} \tag{6}$$

The equation is further simplified through a scaling analysis in which variations in the x-direction are assumed to occur over length scales L_x. Perturbation solutions of the resulting equations for cases with L_x=1 cm and L_x=10 cm are derived in appendix A. In both scaling regimes, we find that the path of the light ray is given explicitly in terms of the squared buoyancy frequency by

$$z(x) = z_i + x\cot\phi_i - \gamma\int_0^x\int_0^{\hat{x}} N^2\left(\hat{\hat{x}}\right)\,\mathrm{d}\hat{\hat{x}}\mathrm{d}\hat{x}. \tag{7}$$

where z_i is the initial height, and ϕ_i the initial angle of the ray as it enters the stratified fluid.

Repeatedly applying Snell's law, we determine the path of a ray of light from the camera to the tank, which then arcs through the stratified fluid and finally reaches the object image at a height Z above the camera. (Of course, the light itself physically travels from the object image to the camera, but back-tracing the path is geometrically more convenient.) As a function of the local squared buoyancy frequency in the tank $N^2(x)$ and the (small) angle $_0$ to the horizontal at which the light ray is incident upon the camera, the total vertical rise of the light ray is

$$\begin{aligned} Z\left(N^2,\phi_0\right) \simeq\ & L_c\phi_0 + L_t\frac{n_a}{n_0}\phi_0 - \gamma\int_0^{L_t}\int_0^x N^2(\hat{x})\mathrm{d}\hat{x}\,\mathrm{d}x \\ & + L_s\phi_0 - L_s\frac{n_0}{n_a}\gamma\int_0^{L_t} N^2(x)\mathrm{d}x. \end{aligned} \tag{8}$$

Here n_a=1 is the refractive index of air. We do not account for factors describing light rays traversing the thickness of the tank walls because their contribution is negligibly small.

We now assume that the squared buoyancy frequency can be decomposed into steady state and perturbation terms. Explicitly, we write $N^2=N_0^2+\Delta N^2$, where $\Delta N^2 \equiv -(g/\rho_0)\partial\rho/\partial z$ is the change in the squared buoyancy frequency due to waves as measured by the vertical derivative of the perturbation density field ρ. Although ΔN^2 is generally a function of three-dimensional space and time, for the purposes of calculating displacements of a single light ray at a fixed instant, we take ΔN^2 to be a function of the across-tank distance x alone.

Substituting into Eq. (8) and subtracting the value of Z in the unperturbed state from the perturbed state, the deflection of a light ray because of changes in the squared buoyancy frequency is

$$\Delta z = -\gamma n_w\left\{L_s\frac{n_w}{n_a}\int_0^{L_t}\Delta N^2(x)\mathrm{d}x + \int_0^{L_t}\int_0^x \Delta N^2(\hat{x})\mathrm{d}\hat{x}\mathrm{d}x\right\}. \tag{9}$$

For the special case in which ΔN^2 is constant, this equation is the same as that derived by Sutherland et al. (1999) in their study of waves generated by an oscillating cylinder (although, for completeness, they included effects of the tank walls.)

3.2 Discretization of the problem

In practise, an array of values $\Delta z(y,z)$ is measured in experiments. By inverting Eq. (9), we are able to determine the amplitude of the waves in terms of the $\Delta N^2(x,y,z)$ field. If the wave field were fully three dimensional, finding ΔN^2 would require views from many angles to reconstruct the wave field accurately. However, in oscillating sphere experiments a single perspective suffices because the internal waves are axisymmetric, and therefore they appear identical from all angles.

In this section, the procedure used to determine ΔN^2 from Δz for axisymmetric waves is described. In order to focus on the key concepts, we consider one quadrant of a horizontal "slice" through the wave field at some arbitrary height z_s above the sphere, with the sphere itself at the origin. We define $\Delta z_s(y) \equiv \Delta z(y,z_s)$ and, exploiting axisymmetry, we assume that at a fixed vertical level ΔN^2 is a function of $R=(x^2+y^2)^{1/2}$.

Employing tomographic inversion techniques, we convert the integral formula for Δz into a matrix equation that we may then invert. Thus $\Delta z_s(y)$ is represented by the M-component vector

$$\Delta\mathbf{z}_s = (\Delta z_s(y_1), \Delta z_s(y_2), \ldots, \Delta z_s(y_M)),$$

in which $y_i=(i+1/2)\Delta y$ is the horizontal location of the midpoint of each pixel in the object image from which $\Delta z_s(y_i)$ is determined. In discretized form, $\Delta N^2(R)$ is modelled by a sequence of concentric rings each of width ΔR. Explicitly, we represent $\Delta N^2(R)$ by the $(M+1)$-component vector

$$\Delta\mathbf{N}^2 = \left(\Delta N^2(R_0), \Delta N^2(R_1), \ldots, \Delta N^2(R_M)\right),$$

in which $R_j=(j+1/2)\Delta R$ is the average of the inner and outer radii of the j'th ring. Typically, we choose ΔR to have the same horizontal resolution as Δy.

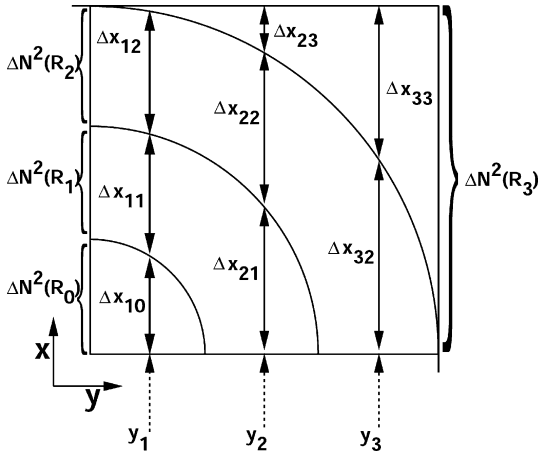

Fig. 3. Schematic of mesh and notations used to discretise the integrals in Eq. (9)

We then consider the path of M equally spaced rays that traverse in the x-direction through the rings, as shown schematically for the case M=3 in Fig. 3. Thus we find

$$\int_0^L \Delta N^2(R)\mathrm{d}x \simeq \sum_{j=i-1}^{M} \Delta N^2\big(R_j\big)\Delta x_{ij} \equiv G_1 \Delta N^2. \tag{10}$$

and

$$\int_0^L \int_0^x \Delta N^2(R)\mathrm{d}\hat{x}\,\mathrm{d}x \simeq \sum_{k=i-1}^{M} \Delta x_{ik} \sum_{j=i-1}^{k} \Delta x_{ij} \Delta N^2\big(R_j\big) \equiv G_2 \Delta N^2. \tag{11}$$

In these expressions, Δx_{ij} is the distance traveled by ray i across ring j, with Δx_{ij}=0 if $j<i$. The distances are determined explicitly by simple geometrical arguments. The elements of the matrix $\mathbf{G}_2$ are given in the compact form

$$g_{ij} = \begin{cases} \Delta x_{i(j-1)}\big(\Delta x_{i(j-1)} + \cdots + \Delta x_{iM}\big) & \text{if } i \le j \le M, \\ 0 & \text{if } 0 \le j \le i. \end{cases} \tag{12}$$

Combining these results, the discrete form of Eq. (9) is obtained

$$\Delta z_s = \eta(\zeta G_1 + G_2)\Delta N^2 \equiv \mathbf{G}\Delta N^2, \tag{13}$$

in which G has dimensions $M\times(M+1)$, and $\eta=-\gamma \mathrm{n_w}$ and $\zeta=L_s(n_w/n_a)$ are both constants. We have so far considered the passage of light rays through half the width of the tank. Using symmetry arguments, G is modified to account for the passage of rays passing through semicircular segments of the rings.

Additional factors may lead to modifications of G and ΔN^2. Because part of the field of view is blocked by the sphere, we discard all rings obstructed by the sphere from the tomography problem. We furthermore assume that ΔN^2 in the largest ring is only negligibly perturbed. More specifically, by using the method of Lagrange multipliers (e.g. see Menke (1983), Sect. 3.10), we specify ΔN^2=0 in the outermost ring.

3.3 Inversion methods

The discrete problem given by Eq. (13) is solved for ΔN^2 in terms of Δz_s by inverting G. Fortunately, with a small number of restrictions we are able to ensure that G is a nonsingular matrix so that standard numerical inversion methods may be applied. One restriction is that at any vertical level we determine ΔN^2 so that it has the same resolution as Δz_s. Because there are no missing elements of Δz_s the inversion problem is not under-determined. In principle, we could acquire Δz_s values both to the right and left of the sphere. By assuming symmetry we are able to reconstruct ΔN^2 by analyzing data only on the right of the sphere. Thus the inversion problem is not over-determined.

Typically we take M=512, the number of horizontal pixels in the original digitized object image of the experiment. The matrix inversion program, which uses standard LU decomposition routines (Press et al. 1993), is repeated for each row of data at 480 different vertical levels z_s. Thus the $\Delta N^2(R,z)$ field is reconstructed from the $\Delta z(x,z)$ data. The C program runs on one 195-MHz, R10 K CPU of a server (SGI Origin2000). The processing of a single 512×480 array takes less than 10 min.

In future work, inversion methods will be applied to reconstruct a fully three-dimensional ΔN^2 field from multiple arrays, each determined from different perspectives through the tank. In general, such inversion problems are likely to be over-determined in some regions and under-determined in others. Generalized inversion methods (Ben-Israel and Greville 1974) may be brought to bear in these circumstances.

3.4 Determination of basic state fields

The ΔN^2 field is determined from Δz, the apparent displacement of lines in an object image compared with the initial unperturbed object image. By comparing two images taken a short time Δt apart, an estimate of the time derivative of the Δz field can be found. Thus the time derivative of the ΔN^2 field can be found: $N^2{}_t$. From these two fields, linear theory can be used to estimate the basic state fields of velocity, perturbation density and vertical displacement (Sutherland et al. 1999).

In particular, the vertical displacement field is determined from the $N^2{}_t$ field using the following relationship from linear theory:

$$N_t^2 = -N^2 \frac{\partial^2 \xi}{\partial z \partial t} = \mathrm{i}\omega N^2 \frac{\partial \xi}{\partial z}. \tag{14}$$

4 Results

Figure 4 shows the ΔN^2 field determined from the Δz field shown in Fig. 2d. The corresponding $N^2{}_t$ field is computed from the difference of two Δz fields taken a short time apart.

As a test of synthetic schlieren, measurements taken using a conductivity probe at a series of points on the upper right-hand flank of the oscillating sphere are

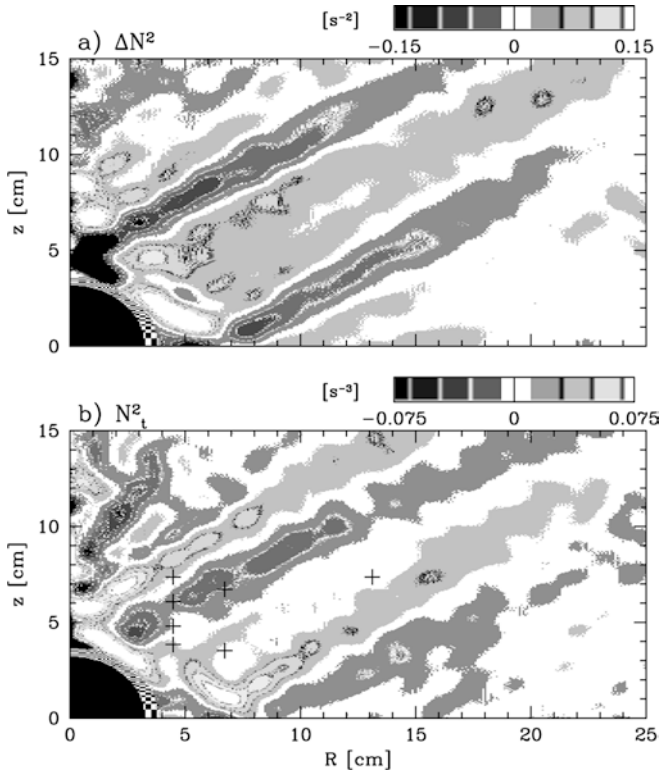

Fig. 4. Plots of **a)** ΔN^2 and **b)** N_t^2 determined from the Δz field shown in Fig. 2d. In b) indicate positions of direct measurements taken by the conductivity probe (see Table 1)

compared with measurements taken using synthetic schlieren. In a single experiment, the probe measures conductivity variations at a point in space over time. From calibration measurements, these are transformed to density variations $\rho(t)$ and, knowing the background density gradient ($d\rho/dz$), these are in turn transformed to measurements of vertical displacement ξ using

$$\xi = -(d\bar{\rho}/dz)^{-1}\rho. \qquad (15)$$

Because the signal variations are small (only a few times greater than the probe resolution), a Gaussian weighted smoothing procedure is used recreate the continuous signal. Thus we estimate the amplitude $A_\xi^{(p)}$ of the vertical displacement field to an accuracy of 0.02 cm.

To find the corresponding amplitude from schlieren measurements, we reduce errors from signal noise by finding the root-mean-square average of the N^2_t field determined for 16 different times during one period of oscillation. Multiplying by $2^{1/2}$, the resulting field gives the amplitude envelope of the N^2_t field. At each position of the probe, we extract the corresponding amplitude $A_{N_t^2}$. To find the amplitude of the vertical displacement field we use Eq. (14) and estimate that the vertical derivative can be replaced by the characteristic inverse vertical scale $2\pi/(2a/\sin\Theta)$. Thus

$$A_\xi^{(s)} \simeq A_{N_t^2}\frac{a}{\pi}\frac{2}{N^3\sin(2\Theta)}, \qquad (16)$$

in which $\Theta=\cos^{-1}(\omega/N)$ is the angle between the wave beam and the vertical axis through the centre of the sphere.

Values of $A_\xi^{(p)}$ and $A_\xi^{(s)}$ measured by the probe and synthetic schlieren, respectively, are listed in Table 1. Except near the sphere, the actual vertical displacement field is much smaller than the probe's resolution. Therefore probe measurements serve as only as crude validation of schlieren measurements.

For the purposes of examining the structure of the upper conical-shaped wave beam, it is convenient to define an orthogonal along-beam (r) and across-beam (σ) coordinate system, in which the r -axis passes through the center of the sphere at an angle Θ to the vertical, and σ increases as z increases (Sutherland and Linden 2002).

The amplitude envelope determined in three experiments is illustrated here by the normalized ΔN^2 field: $\langle\Delta N^2\rangle/A_{N^2}$. We use the normalisation factor $A_{N^2} = N^2A/a$ so that, in linear theory, the curves should overlap independent of the amplitude of oscillation.

Figure 5 shows along-beam cross sections taken along the centre of the wave beam (σ=0) and along the upper flank of the wave beam (σ=+a). To within the error determined by the fluctuation of the curves, the normalised amplitudes are the same. This shows that nonlinear effects are negligible even for relative amplitudes as large as $A/a\simeq0.27$. Comparing the two plots, one sees that along the centreline of the wave beam (σ=0) the amplitude first decreases then increases, whereas the amplitude decreases approximately monotonically at the flanks of the wave beam (σ=a). For $r/a\geq7$, the amplitude is larger along the centreline. These results are consistent with observations of waves generated by an oscillating cylinder (Sutherland et al. 1999; Sutherland and Linden 2002) in which a bimodal wave beam near the source became a unimodal wave beam far from the source as a result of viscous attenuation.

The across-beam plots in Fig. 6 explicitly show the bimodal structure of the waves near the sphere. The

Table 1. Comparison of vertical displacements measured by conductivity probe and by synthetic schlieren in an experiment with $2A$=1.74 cm

Probe position		Probe measurement $A_\xi^{(p)}/A$	Schlieren measurement $A_\xi^{(s)}/A$
(R/a, z/a)	(r/a, σ/a)		
(1.4, 1.2)	(2.1, 0.5)	0.065±0.023	0.108±0.011
(1.4, 1.5)	(2.4, 0.8)	0.083±0.023	0.108±0.022
(1.4, 1.9)	(2.6, 1.0)	0.081±0.023	0.130±0.029
(1.4, 2.3)	(2.9, 1.4)	0.073±0.023	0.129±0.013
(2.1, 1.1)	(2.6, 0.2)	0.050±0.023	0.062±0.014
(2.1, 2.1)	(3.4, 1.0)	0.064±0.023	0.126±0.022
(4.1, 2.3)	(5.3, 0.4)	0.027±0.023	0.044±0.011

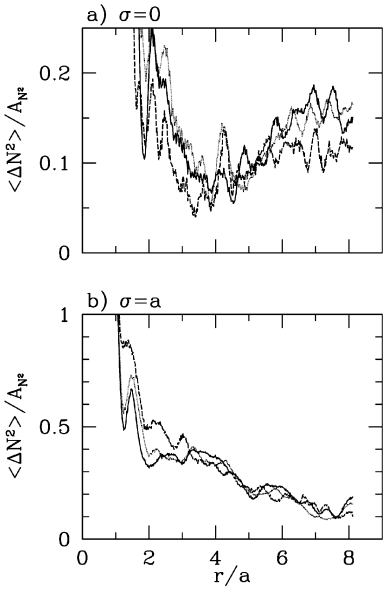

Fig. 5 a,b. Profiles of the normalised $<\Delta N^2>$ field determined in three experiments from along-beam slices at: **a)** σ=0. **b)** σ=a. Profiles are shown for experiments with A/a=0.27 (solid line), A/a=0.18 (short-dashed line) and A/a=0.10 (long-dashed line)

profiles are taken at a radial distance of r/a=5, which is sufficiently far from the sphere that the overlap between the upward and downward propagating wave fields is not dominant.

5 Conclusions

We have adapted synthetic schlieren to measure the amplitude of axisymmetric waves. As well as being nonintrusive, a significant advantage of this method is its extreme sensitivity: in our experiments, displacements because of internal waves as small as 0.01 cm were measured. In a larger tank, even smaller amplitudes could be measured provided the distance along which light rays are deflected by the disturbance is sufficiently long.

This work constitutes a first step towards adapting synthetic schlieren to measure fully three-dimensional wave fields. In general, this would require multiple perspectives of the waves and more sophisticated inverse tomographic techniques. If successful, however, it would provide a powerful new tool for measuring small-amplitude internal waves generated by complex topography and turbulence.

Scaling analysis

Here we give a detailed explanation of how the approximate solution to Eq. (6), given by Eq. (7), has been obtained through scaling and perturbation analysis. Equation (6) is simplified by dropping terms that are revealed to be small by a scaling analysis. In the x-direction, we expect variations on scales L_x, which is on the order of the sphere radius, on the order 1–10 cm in our

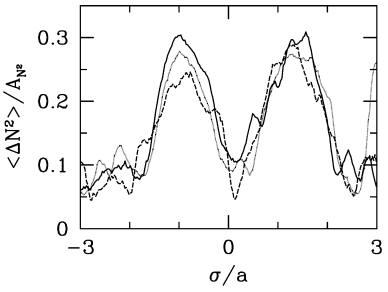

Fig. 6. As in Fig. 5 but showing across-beam slices at r/a=5

experiments. In the z-direction, the length scale L_z is set to the vertical distance traveled by a ray as it progresses from the front to the back of the tank. In typical experiments, $L_z \simeq 1$ cm, $N_0^2 \sim 1$ s^{-2} and $\gamma \sim 10^{-4}$ s^2/cm. We transform to nondimensional variables (denoted by tildes) with the substitutions $(x, z) = (L_x\tilde{x}, L_z\tilde{z})$, $\alpha_0 = n_0\tilde{n}$ and $\alpha_1 = -\gamma n_0 N_0^2 \widetilde{N^2}$. Thus Eq. (6) becomes

$$\frac{L_z}{L_x^2}\tilde{z}'' + \gamma^2 N_0^4 L_z \frac{\widetilde{N^4}}{\tilde{n}^2}\tilde{z} - \frac{L_z^3}{L_x^2}\gamma^2 N_0^4 \frac{\widetilde{N^2}\widetilde{N^2}'}{(\tilde{n}')^2}\tilde{z}''\tilde{z}'\tilde{z} - \frac{L_z^2}{L_x^2}\gamma N_0^2 \frac{\widetilde{N^2}}{\tilde{n}}\tilde{z}''\tilde{z}' = -\gamma N_0^2 \frac{\widetilde{N^2}}{\tilde{n}}. \tag{17}$$

Substituting typical characteristic scales and supposing first that $L_x \sim 1$ cm, we obtain

$$\tilde{z}'' + 10^{-8}\frac{\widetilde{N^4}}{\tilde{n}^2}\tilde{z} - 10^{-8}\frac{\widetilde{N^2}\widetilde{N^2}'}{(\tilde{n}')^2}\tilde{z}''\tilde{z}'\tilde{z} - 10^{-4}\frac{\widetilde{N^2}}{\tilde{n}}\tilde{z}''\tilde{z}' = -10^{-4}\frac{\widetilde{N^2}}{\tilde{n}}. \tag{18}$$

The leading order equation is

$$\frac{\mathrm{d}^2\tilde{z}^{(0)}}{\mathrm{d}\tilde{x}^2} = 0, \tag{19}$$

with solution

$$\tilde{z}^{(0)} = z_i + \tilde{x}\cot\phi_i, \tag{20}$$

where z_i refers to the initial height of the ray and $_i$ refers to its angle as it enters the stratified medium.

At next order, ϵ=10^{-4}, perturbation theory with $z \simeq \tilde{z}^{(0)} + \varepsilon\tilde{z}^{(1)}$ gives the equation

$$\frac{\mathrm{d}^2\tilde{z}^{(1)}}{\mathrm{d}\tilde{x}^2} + \frac{\tilde{N}^2}{\tilde{n}}\frac{\mathrm{d}^2\tilde{z}^{(0)}}{\mathrm{d}\tilde{x}^2}\frac{\mathrm{d}\tilde{z}^{(0)}}{\mathrm{d}\tilde{x}} = -\frac{\tilde{N}^2}{\tilde{n}}. \tag{21}$$

Using Eq. (19), the solution is found:

$$\tilde{z}^{(1)} = -\int_0^{\tilde{x}}\int_0^{\tilde{\tilde{x}}}\frac{\tilde{N}^2\left(\tilde{\tilde{\tilde{x}}}\right)}{\tilde{n}\left(\tilde{\tilde{\tilde{x}}}\right)}\mathrm{d}\tilde{\tilde{\tilde{x}}}\mathrm{d}\tilde{\tilde{x}}. \tag{22}$$

Repeating this procedure but supposing $L_x \simeq 10$ cm gives the equation

$$\tilde{z}''+10^{-6}\frac{\widetilde{N^4}}{\tilde{n}^2}\tilde{z}-10^{-8}\frac{\widetilde{N^2}\widetilde{N^2}'}{(\tilde{n}')^2}\tilde{z}''\tilde{z}'\tilde{z}$$
$$-10^{-4}\frac{\widetilde{N^2}}{\tilde{n}}\tilde{z}''\tilde{z}'=-10^{-2}\frac{\widetilde{N^2}}{\tilde{n}}. \quad (23)$$

The leading order equation is again given by Eq. (19). At next order, $\epsilon=10^{-2}$, the corresponding equation for $\tilde{z}^{(1)}$ is identical to Eq. (21) after using Eq. (19).

Therefore, for waves with horizontal scales ranging between 1 and 10 cm, we find

$$z \simeq z_i + x\cot\phi_i - \gamma n_0 \int_0^x \int_0^{\hat{x}} \frac{N^2\left(\hat{\tilde{x}}\right)}{n\left(\hat{\tilde{x}}\right)} \mathrm{d}\hat{\tilde{x}}\mathrm{d}\hat{x}. \quad (24)$$

Finally, we note that variations in the refractive index occur on the order $\Delta n/n\sim10^{-5}$, whereas typical changes in the buoyancy frequency due to waves occur on the order $\Delta N^2/{N_0}^2\sim10^{-1}$ to 10^{-2}. Thus, we can treat $n(x)$ as approximately constant in the denominator in Eq. (24) to give Eq. (7).

References

Appleby JC, Crighton DG (1987) Internal gravity waves generated by oscillations of a sphere. J Fluid Mech 183:439–450

Ben-Israel A, Greville TNE (1974) Generalized inverses: theory and applications. Wiley, New York

Dalziel SB (1992) Decay of rotating turbulence: some particle tracking experiments. Appl Sci Res 49:217–244

Dalziel SB, Hughes GO, Sutherland BR (2000) Whole field density measurements. Exp Fluids 28:322–325

Greenberg PS, Klimek RB, Buchele DR (1995) Quantitative rainbow schlieren deflectometry. Appl Optics 34:3810–3822

Irvin BR, Ross J (1991) Observations of pattern evolution in thermal convection with high-resolution quantitative schlieren imaging. Phys Fluids A 3:1699–1710

Lighthill MJ (1978) Waves in fluids. Cambridge University Press, Cambridge

Menke W (1983) Geophysical data analysis. Academic Press, New York

Mowbray DE (1967) The use of schlieren and shadowgraph techniques in the study of flow patterns in density stratified liquids. J Fluid Mech 27:595–608

Mowbray DE, Rarity BSH (1967) A theoretical and experimental investigation of the phase configuration of internal waves of small amplitude in a density stratified liquid. J Fluid Mech 28:1–16

Oster G (1965) Density gradients. Sci Am 213:70–76

Press WH, Flannery BP, Teukolsky SA, Vetterling WT (1993) Numerical recipes: the art of scientific computing, 2nd edn. Cambridge University Press, New York

Stevenson TN (1969) Axisymmetric internal waves generated by a travelling oscillating body. J Fluid Mech 35:219–224

Sutherland BR, Dalziel SB, Hughes GO, Linden PF (1999) Visualisation and measurement of internal waves by "synthetic schlieren". Part 1: Vertically oscillating cylinder. J Fluid Mech 390:93–126

Sutherland BR, Hughes GO, Dalziel SB, Linden PF (2000) Internal waves revisited. Dyn Atmos Ocean 31:209–232

Sutherland BR, Linden PF (2002) Internal wave excitation by a vertically oscillating elliptical cylinder. Phys Fluids 14:721–731

Voisin B (1991) Internal wave generation in uniformly stratified fluids. 1. Green's function and point sources. J Fluid Mech 231:439–480

Weast RC (ed) (1981) Handbook of chemistry and physics, 62nd edn. CRC, Boca Raton